Journal of Applied Mechanics and Technical Physics, Vol. 36, No. 5, 1995

STRENGTH AND DEFORMABILITY OF ZIRCONIUM ALLOY E-110 UNDER SIMPLE AND COMPLEX LOADINGS

I. E. Ginsburg, V. M. Zhigalkin, V. A. Kotrekhov,[1] S. Yu. Zavodchikov,[1] A. F. Lositsky,[1] O. M. Usoltseva, Yu. P. Shevnin

UDC 539.374:621.039.51

The goal of this paper, is to investigate the character of elastoplastic deformation of zirconium alloy E-110 (Zr + 1%Nb) under biaxial tension generated in a thin-walled tubular sample by an axial force and internal pressure under simple and complex loading at room temperature. Particular attention has been given to the study of the features of complex loading, where partial unloading was realized in one of the basic directions of the stress tensor [1–5].

The results of the experimental study of the transformation of the frontal part of the loading surface are given for three series of repeated loadings after a preliminary simple and complex loading along a loading trajectory whose first section represented axial tension, and the second section represented orthogonal loading in the plane of basic stresses. Repeated radial loadings are carried out after three types of unloading: complete unloading along a straight line into the zero stressed state, reverse motion in the second section of the loading trajectory to the break point, and reverse motion along the trajectory of preliminary loading to the zero stressed state. It is shown that the shape of the loading surface is determined by the type of stressed state at the initial moment of repeated loading, by the loading direction, and by the history of unloading. The shapes of the loading surfaces are analyzed in terms of a variant of the plasticity theory for an anisotropically strengthening medium [4, 5].

As in [1–3], data of the experiments on thin-walled tubular samples which made it possible to determine the types of loading trajectories leading to an increase in the strength and deformation properties are presented.

1. Let us consider the results of the experimental investigation of elastoplastic deformation of zirconium alloy E-110. The experiments were carried out on a CH-10 installation designed in the Special Construction–Technical Bureau at the Institute of Strength Problems of the Ukrainian Academy of Sciences (Kiev).

Standard tubes from a common supply with the following sizes were used as test samples: outside diameter $D = 13.58 \mp 0.05$ mm, inside diameter $d = 11.70 \mp 0.05$ mm, working part length $L = 170 \mp 1.0$ mm. The following parameters were recorded during the tests: axial force, internal pressure, axial displacement on a given base, and external diameter.

The loading stability was ensured by permanent control of the operating conditions of the testing machine. The loading trajectories were given in the space of basic stresses and have the shape of one-link and multi-link broken lines. A loading rate of $\dot{\sigma} = 0.1$ MPa/sec was chosen to exclude time effects under inelastic deformation, which are practically not recorded in the case of low velocities of loading ($\dot{\sigma} \leqslant 0.1$ MPa/sec) [4].

Let us consider the stress state of a material element with fixed basic directions of the stress tensor: $\sigma_1 \geqslant \sigma_2 \geqslant \sigma_3$. The basic tangential stresses $2T = \sigma_1 - \sigma_3$, $2T_{12} = \sigma_1 - \sigma_2$, $2T_{23} = \sigma_2 - \sigma_3$ $\quad (T = T_{12} + T_{23})$

Mining Institute, Siberian Division, Russian Academy of Sciences, Novosibirsk 630091. [1]Industrial Association Chepetsk Machine Plant, 427600 Glazov. Translated from Prikladnaya Mekhanika i Tekhnicheskaya Fizika, Vol. 36, No. 5, pp. 67–80, September–October, 1995. Original article submitted March 17, 1994; revision submitted October 11, 1994.

0021-8944/95/3605-0697 $12.50

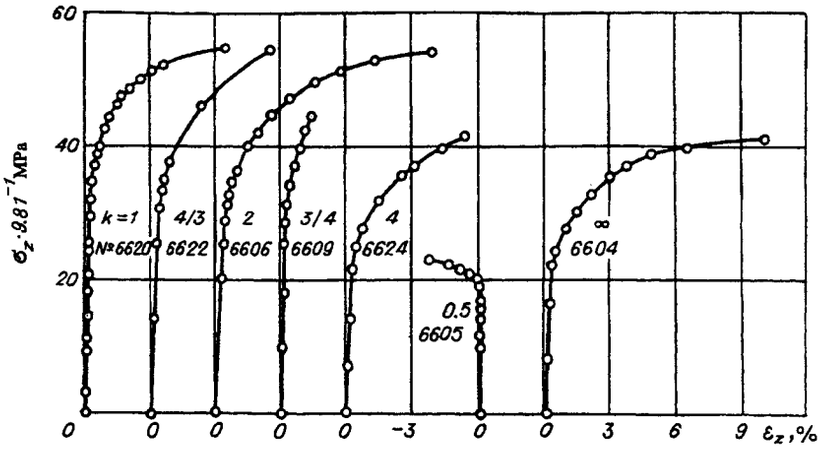

Fig. 1

are related by the Lode parameter μ_σ:

$$T\mu_\sigma = T_{23} - T_{12}.$$

For the increments of these tangential stresses $2\Delta T = \Delta\sigma_1 - \Delta\sigma_3$, $2\Delta T_{12} = \Delta\sigma_1 - \Delta\sigma_2$, $2\Delta T_{23} = \Delta\sigma_2 - \Delta\sigma_3$ a parameter in the form of additional loading $\mu_{\Delta\sigma}$ [4] is introduced:

$$\Delta T\mu_{\Delta\sigma} = \Delta T_{23} - \Delta T_{12}.$$

The results of the experimental investigations are analyzed in terms of the plasticity theory for an anisotropically strengthening medium [4, 5], according to which plastic deformation is represented as a sequence of plastic slidings (shears) in the planes of action of the basic tangential stresses T, T_{12}, and T_{23} which are called sliding areas T, T_{12}, and T_{23} (T are the areas of the basic shear if the tangential stresses are related by the inequalities $T \geqslant T_{12} \geqslant T_{23}$ or $T \geqslant T_{23} \geqslant T_{12}$).

2. The experimental data presented below are divided into two groups. The first group contains the results of analysis of the elastoplastic deformation of the alloy under proportional loadings and complex loadings at a constant value of the maximal tangential stress (T = const). Active loadings take place in this section over the slide areas T and T_{23}, partial unloading — over the areas T_{12} with the cessation of growth of plastic shears, and partial strengthening occurs in the direction of unloading [5]. Direct and reverse loading was made in the section T = const, and at the end of the section of complex loading, the value of the second basic stress σ_2 considerably exceeded the value of the first basic stress σ_1. The influence of the sections of direct and reverse loading on the subsequent character of the alloy strengthening under complex loading is studied, in which case the state of pure torsion with superimposed hydrostatic pressure is realized, and the increments of the tangential stresses are $\Delta T_{23} = 2\Delta T = -2\Delta T_{12} \geqslant 0$, $\mu_{\Delta\sigma} = 3$.

The degree of the initial anisotropy was investigated by testing samples under proportional loadings. Experimental data are necessary to determine the initial strength and deformation characteristics.

Figures 1 and 2 illustrate the results of the tests in the form of strain diagrams for the dependence of the axial tension σ_z on the axial strain ε_z [$\sigma_z = \sigma_z(\varepsilon_z)$], and the dependence of the circumferential tension σ on the circumferential strain ε_φ [$\sigma_\varphi = \sigma_\varphi(\varepsilon_\varphi)$] (the sample number and the ratio of basic tensions $k = \sigma_z/\sigma$ are indicated at the lines). The loading trajectories are given in Fig. 3 on the dimensionless plane of variables $\sigma_z/\sigma^s_{0.2} - \sigma_\varphi/\sigma^s_{0.2}$ ($\sigma^s_{0.2}$ is the yield stress of the alloy at axial tension corresponding to a tolerance for the residual plastic strain $\varepsilon^p_z = 0.2\%$).

Table 1 presents the main mechanical characteristics of the alloy obtained in the tests of the samples: sample number, ratio of basic tensions k, the Lode parameter

$$\mu_\sigma = \frac{2\sigma_2 - \sigma_1 - \sigma_3}{\sigma_1 - \sigma_3}$$

TABLE 1

Sample number	$k = \sigma_z/\sigma_\varphi$	μ_σ	$\sigma_1 \cdot 9.81^{-1}$ MPa			$\alpha_z \cdot 10^{-2}$ MPa	$\alpha_\varphi \cdot 10^{-2}$ MPa
			$\sigma^s_{0.2}$	$\sigma^s_{0.5}$	$\sigma^s_{1.0}$		
6601	∞	−1.0	23.8	26.5	29.0	66.50	
6624	4	−0.5	24.8	28.0	30.5	70.13	−33.50
6606	2	0	32.3	36.0	39.5	65.68	−14.00
6622	4/3	0.5	34.6	38.2	41.0	83.85	−20.50
6620	1	1	36.0	40.8	45.5	132.00	+210.00
	1	1.0	47.5	53.5	55.5		
6609	3/4	0.5	46.2	49.5	51.2	105.00	167.00
6605	0.5	0	41.8	44.5	45.8	352.00	147.00

($\sigma_3 = \sigma_r$ is the radial tension equal to zero, the tensions σ_1, σ_2 take the values σ_z or σ_φ depending on the ratio of tensions k), the yield stresses $\sigma^s_{0.2}$, $\sigma^s_{0.5}$, $\sigma^s_{1.0}$ corresponding to the values of plastic strain in the first basic direction $\varepsilon^p_1 = 0.2,\ 0.5,\ 1.0\%$, elastic constants $\alpha_z = \Delta\sigma_z/\Delta\varepsilon_z$, $\alpha_\varphi = \Delta\sigma_\varphi/\Delta\varepsilon_\varphi$ ($\Delta\varepsilon_z$, $\Delta\varepsilon_\varphi$) are the increments of elastic deformations in the axial and circumferential directions, respectively.

The test data given in Figs. 1 and 2 and in Table 1 indicate the initial anisotropy of the alloy, which is a consequence of the technology for manufacturing the shells of heat-generating elements and technological channels [7, 8]. The diagrams of deformation of the alloy in the first and second basic directions, corresponding to the same value of the Lode parameter μ_σ but to different ratios of tensions k, do not coincide with each other. The elastic constants α_z, α_φ are also different. In the direction of rolling (axial direction) these values are smaller than in the transverse direction. The yield stress depends on the ratio of tensions k.

The data of the tests obtained under equal biaxial tension $\sigma_z = \sigma_\varphi$ should be mentioned. The onset of yield in the axial direction occurred earlier than in the circumferential direction. Therefore, for this case, Table 1 presents two yield stresses corresponding to the given plastic strain ε^p_1, in the form of a fraction, the numerator of which is the yield stress in the axial direction, and the denominator is the yield stress in the circumferential direction.

Figure 3 gives initial curves of the yield of the alloy in the plane of variables $\sigma_z/\sigma^s_{0.2} - \sigma_\varphi/\sigma^s_{0.2}$. They were constructed to the above-mentioned tolerances for residual plastic strain $\varepsilon^p_1 = \text{const}$. Seven loading trajectories are presented. Points corresponding to different values of ε^p_1 are marked on each of them. Points 1, 2 on the loading trajectory $\sigma_z = \sigma_\varphi$ correspond to $\varepsilon^p_z = \text{const}$, $\varepsilon^p_\varphi = \text{const}$. Curves of constant values of ε^p_1 are drawn through points 1.

The curves of constant values ε^p_1 shown in Fig. 3 are not instantaneous yield curves. By the yield curve is meant a line separating the elastic area from the plastic area. The curves $\varepsilon^p_1 = \text{const}$ can be used as practical indices of the plastic behavior of the alloy in the first basic direction under proportional biaxial tension.

It should be noted that there are practically no experimental data in the literature on the elastoplastic deformation of the alloy under simple and complex loadings [9, 10].

Let us consider the results of the tests under complex loading ($T = \text{const}$). It is convenient to represent the loading trajectory in the deviator plane of variables of A. A. Il'yushin:

$$S_1 = \sqrt{\frac{2}{3}}\left(\sigma_1 - \frac{1}{2}\sigma_2\right), \quad S_2 = \frac{1}{\sqrt{2}}\sigma_2, \qquad |\mathbf{S}| = S = \sqrt{S_1^2 + S_2^2} = \sqrt{\frac{2}{3}}\sigma_i.$$

Here $\mathbf{S}$ is the vector of stresses, and σ_i is the intensity of stresses. Figure 4 presents the loading trajectory $OABAC$, the first section OA of which is the axial tension $\sigma_z > 0$, $\sigma_\varphi = 0$ to $\sigma_z = 1.17\sigma^s_{0.2}$ ($\sigma^s_{0.2}$ is the yield stress of the alloy under axial tension: $\sigma^s_{0.2} = 235$ MPa).

Let us keep the notation of basic stresses and deformations in accordance with their directions at the end of the first section OA; then $\sigma_1 = \sigma_z$, $\sigma_2 = \sigma_\varphi$, $\varepsilon_1 = \varepsilon_z$, $\varepsilon_2 = \varepsilon_\varphi$.

Figure 4 shows that these is a sharp inflection of the loading trajectory at point A at an angle of 120°

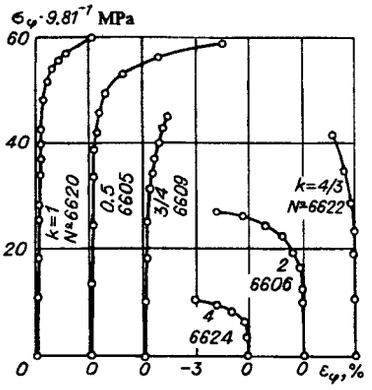

Fig. 2

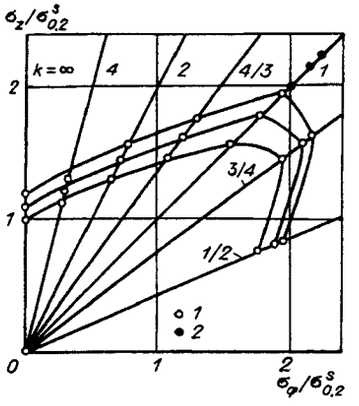

Fig. 3

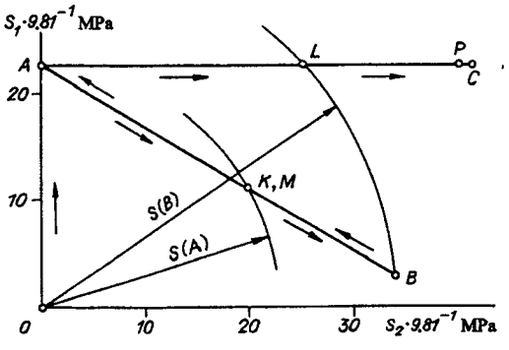

Fig. 4

that goes over into section AB, in which loading takes place at a constant value of the axial tension $\sigma_z = \sigma_z(A)$ [$\sigma_z(A)$ is the axial tension at point A] and $\sigma_\varphi > 0$ to the value of the circumferential tension σ_φ at point B [$\sigma_\varphi(B) = 491$ MPa]. At point B at the end of the section of complex loading $k = 0.583$, $\mu_\sigma = 2.429$. Reverse loading is realized in section BA. At point A, there is again an abrupt inflection of the trajectory at an angle of 90° that goes over into section AC of complex loading, in which the increments of stresses are related as $\Delta\sigma_\varphi = 2\Delta\sigma_z$, $\Delta T_{23} = 2\Delta T = -2\Delta T_{12} > 0$, $\mu_{\Delta\sigma} = 3$. Point C corresponds to the moment preceding failure of the sample.

Figure 5 presents strain diagrams $\sigma_z = \sigma_z(\varepsilon_z)$, $\sigma_\varphi = \sigma_\varphi(\varepsilon_\varphi)$ (points 1) for the loading trajectory shown in Fig. 4. The experimental data indicate the following. In section OA of the loading trajectory the material element is brought into a plastic state — the state of complete plasticity — by means of axial tension. The plastic deformation is a result of shears in the sliding areas T and T_{12}, $T = T_{12}$.

Additional loading from point A in section AB of the loading trajectory causes elastic strain of the element in the circumferential direction [as is evident from the plot $\sigma_\varphi = \sigma_\varphi(\varepsilon_\varphi)$ in Fig. 5]. The slope of the curve in section AK coincides with the elastic slope of the pure shear curve $\sigma_\varphi = \sigma_\varphi(\varepsilon_\varphi)$ obtained from the experimental data at biaxial tension $\sigma_z = 0.5\sigma_\varphi$, $\mu_\sigma = 0$ (see Fig. 2). A noticeable deviation of the curve from the elastic curve is observed in the vicinity of point K.

Let us elucidate the character of elastoplastic deformation of the element in the axial direction under additional loadings in section AB of the trajectory. For this purpose, points of the dependence of the circumferential stress on the axial strain $\sigma_\varphi = \sigma_\varphi(\Delta\varepsilon_z)$ (points 2) are marked in section ABA of the curve $\sigma_z = \sigma_z(\varepsilon_z)$. It is seen that a linear dependence is clearly traced in section AK; a deviation from this

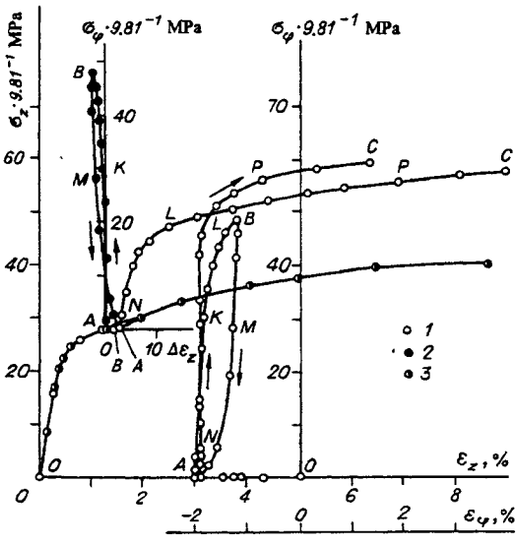

Fig. 5

dependence is observed at point K, which means replacement of elastic deformation by plastic deformation.

Thus, additional loading from point K of the loading trajectory in Fig. 4 causes the simultaneous appearance of plastic deformation in the axial and circumferential directions, and point K is a boundary between the elastic state and the state of complete plasticity. Plastic shears take place simultaneously over the sliding areas T and T_{23}. It should be noted (as is seen from Fig. 4) that the modulus of the stress vector $|\mathbf{S}| = S$ at point K is equal to the value of the stress vector at point A $S(A)$ with accuracy up to the spread in the experimental data. The intersection point of the circular arc of radius $S(A)$ and straight line AB in Fig. 4 can be reasonably considered the boundary between the elastic state and the state of complete plasticity on the deviator plane of A. A. Il'yushin (S_1, S_2).

The loadings $\sigma_\varphi > 0$, $\sigma_z = \sigma_z(A)$ in section AB of the loading trajectory cause, one after another, the following deformation states:

— elastic state, as long as the intensity of stresses σ_i is less than the intensity of stresses σ_i at the end of the simple loading section;

— complete plasticity state (when the stress σ_i exceeds the value σ_i at the end of the simple loading section). A changeover of sliding areas takes place: the sliding areas T_{23} become the basic shear areas and the sliding areas T become the areas of the second shear. The tangential stresses are related by the inequalities $T_{23} \geqslant T > T_{12}$. The tangential stress T_{12} changes sign, and a changeover from partial unloading to active loading occurs.

Complete unloading takes place in section BA of the loading trajectory, as long as the stress $\sigma_\varphi \geqslant \sigma_z$ and the slide areas T_{23} are the areas of basic shear. The stresses $\sigma_\varphi = \sigma_z = \sigma_z(A)$ at points M of the trajectory and the strain diagrams. Additional loading from point M caused the noticeable appearance of plastic deformations in the axial direction. The sliding areas T again become the basic shear areas. The deformation in the circumferential direction is elastic. Noticeable plastic deformation and a conversion into the deformed state of complete plasticity with sliding areas T and T_{12} are observed in the vicinity of point A.

Additional loading from point A of the loading trajectory in section AC, as is seen from the strain diagrams in sections AC of Fig. 5, caused elastic deformation in the axial and circumferential directions to point N. Under subsequent additional loadings, a noticeable deviation of the diagram $\sigma_z = \sigma_z(\varepsilon_z)$ from the elastic diagram is observed and deformation in the circumferential direction is elastic. Plastic deformation in a state similar to the incomplete plasticity state is observed in section AL of the loading trajectory. At point L of the trajectory, the value of the stress vector $\mathbf{S}$ is equal to the value of the stress vector at point B at the moment of application of reverse additional loading $S = S(B)$. At point L, the noticeable appearance of

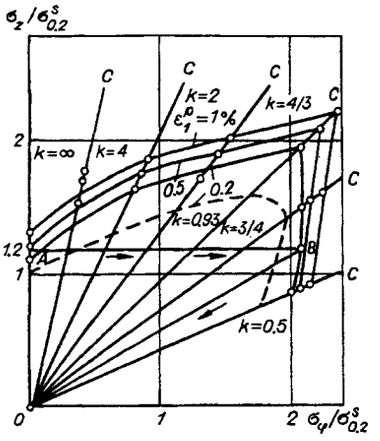

Fig. 6

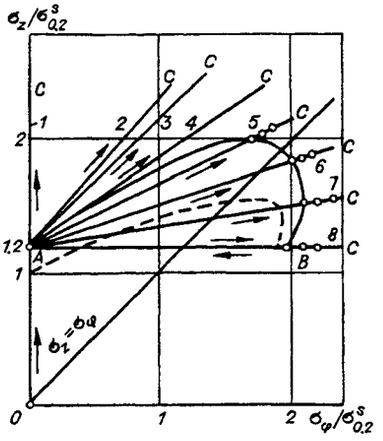

Fig. 7

plastic deformation in the circumferential direction is observed. The material element turns into a deformed state — the state of complete plasticity. The sliding areas are T and T_{23} (T are the areas of basic shear).

Thus, loading in section AC of the loading trajectory causes, one after another, the following deformed states:

— an elastic state,

— a state of incomplete plasticity, as long as the intensity of stresses is less than the intensity of stresses at the end of section AB of complex loading,

— a state of complete plasticity (when σ_i exceeds its value at point B).

At point P, a changeover of the sliding areas T and T_{23} takes place; the areas T_{23} become the areas of basic shear. A transition from partial unloading to active loading occurs in the sliding areas T_{12}.

Points of the curve $\sigma_z = \sigma_z(\varepsilon_z)$ of axial tension (points 3) are marked on the curve $\sigma_z = \sigma_z(\varepsilon_z)$. In section AC, points of the curve $\sigma_z = \sigma_z(\varepsilon_z)$ are considerably higher than points of the axial tension curve. The experimental data in section AC of the loading trajectory indicate an abrupt increase in the yield stress and in the ultimate strength. The yield stress in the axial direction determined to tolerance $\varepsilon^p_1 = 0.2\%$ exceeds the initial value of $\sigma^s_{0.2}$ by a factor of 1.79, which is higher than the ultimate strength by a factor of 1.1. The limiting values: the stress σ_z exceeds the ultimate strength under axial tension by a factor of 1.43, the stress σ_φ is higher than the ultimate strength under axial tension by a factor of 1.48, and the deformation ε_z at the moment preceding failure of the sample is higher than the strain under axial tension.

The increase in the strength properties and conservation or increase in the deformation properties in one of the basic directions of the stress tensor result from direct and reverse loading in one of the sections of complex loading accompanied by partial unloading in one of the directions of preliminary plastic deformation and by cessation of the growth of plastic shears in the direction of unloading, by active loadings and growth of plastic shears in other directions, and by excess of the second basic stress over the first one.

Experimental investigation of elastoplastic deformation of the initially anisotropic alloy under simple and subsequent complex loadings accompanied by partial unloading and cessation of the growth of plastic shears in the direction of unloading enabled us to find of the boundary between the deformed states of incomplete and complete plasticity. Whatever the prehistory of loading and the direction of subsequent complex loading, the boundary of the states is determined by the intensity of the stresses at the inflection point of the loading trajectory at the end of the preceding section of the loading trajectory.

These effects can be used as a technological method for controlling the anisotropy of the metal in tubular members and for designing their specified strength and deformation properties.

3. Let us consider the results of the experimental investigations of transformation of the frontal part of the loading surface for three series of repeated simple and complex loadings after preliminary complex

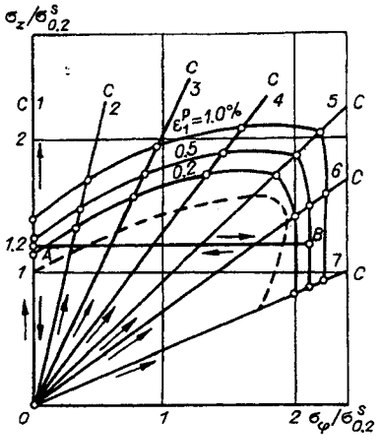

Fig. 8

loading in trajectory OAB (see Fig. 4) and different histories of unloading. The aim of these investigations was to study the influence of preliminary complex loading and of the history of unloading on the character of deformation strengthening of the alloy under repeated loadings. The history of unloading should be taken into account, because partial unloading exists in addition to complete unloading considered conventionally, in which the increments of tangential stresses on the sliding areas T, T_{12}, T_{23} are negative, i.e., $\Delta T < 0$, $\Delta T_{12} < 0$, $\Delta T_{23} < 0$. In this case, under additional loadings unloading takes place in some directions, and active loadings which can cause inelastic deformation or a change in the mechanical state occur in other directions.

The following loading programs were realized:

(1) Loading in trajectory OAB (Fig. 6), unloading in ray BO of simple loading, and repeated simple loading $\sigma_z = k\sigma_\varphi$;

(2) Loading in trajectory OAB, reverse loading in section BA of complex loading to point A (Fig. 7), and repeated complex loading AC from point A in one of the rays, where the parameter of the type of additional loading $\mu_{\Delta\sigma}$ was kept constant;

(3) Loading in trajectory OAB, reverse loading in the trajectory of preliminary loading BAO into the zero stress state, and repeated simple loading $OC\ \sigma_z = k\sigma_\varphi$. The loading trajectories are given in Fig. 8.

In the determination of the yield stress under conditions of repeated loading, a change in the elastic properties resulting from plastic deformation in section OAB of the loading trajectory was taken into account. Young's modulus was reduced by 5–7%, and no change in the Poisson coefficient was observed. The boundary of transition from the elastic into the plastic state was determined to different tolerances for residual plastic strain $\varepsilon^p_1 =$ const in the first basic direction.

Loading in Accordance with Program 1. Figure 6 shows trajectories of preliminary complex loading OAB, of complete unloading BO, and repeated simple loading. Repeated loadings were carried out at different values of k and of the Lode parameter μ_σ: $k = \infty$ ($\mu_\sigma = -1$), $k = 4$ ($\mu_\sigma = -0.5$), $k = 2$ ($\mu_\sigma = 0$), $k = 4/3$ ($\mu_\sigma = 0.5$), $k = 0.93$ ($\mu_\sigma = 1.15$), $k = 3/4$ ($\mu_\sigma = 1.67$), $k = 0.5$ ($\mu_\sigma = 3.0$).

Figures 9 and 10 present sample numbers and strain curves $\sigma_z = \sigma_z(\varepsilon_z)$ and $\sigma_\varphi = \sigma_\varphi(\varepsilon_\varphi)$ in sections $OABO$ of preliminary loading (points 2) and in sections OC of repeated simple loading (points 1). The conditional yield stress was found for radial loading trajectories in the diagrams of deformation $\sigma_1 = \sigma_1(\varepsilon_1)$ as a stress corresponding to tolerances $\varepsilon^p_1 = 0.2$, 0.5, 1.0%. The points in Fig. 6 mark the above-mentioned values of ε^p_1 in the plane of variables $\sigma_z/\sigma^s_{0.2} - \sigma_\varphi/\sigma^s_{0.2}$ in sections OC under repeated simple loadings. Curves of the loading surfaces are drawn through points $\varepsilon^p_1 =$ const. For comparison, the initial yield curve is shown by a dashed line.

Repeated simple loadings of samples subjected to preliminary loading in accordance with program 1 determine the type of loading surface for a given variant of preliminary loading trajectory. The curves

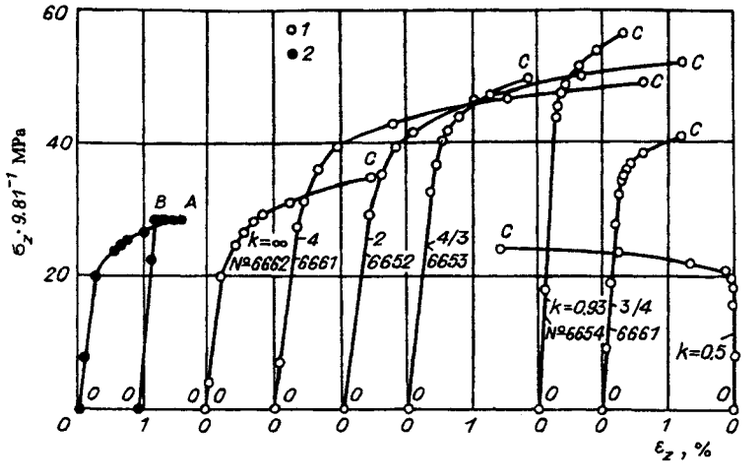

Fig. 9

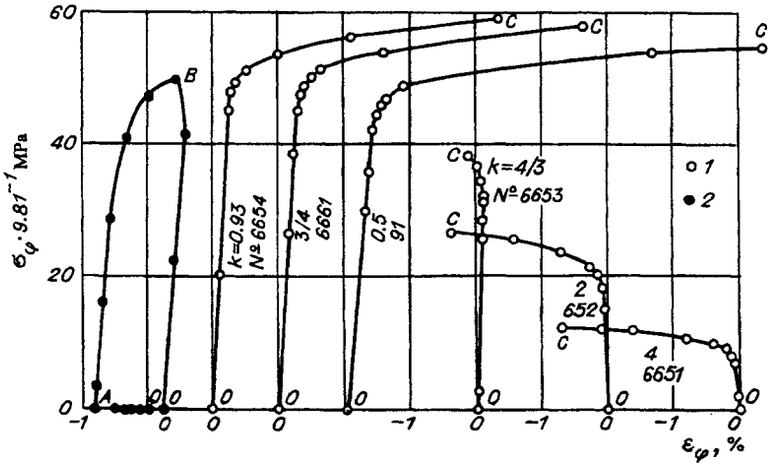

Fig. 10

obtained here to different tolerances ε_1^p indicate the anisotropy of the strengthening process with the greatest strengthening in the direction of preliminary complex loading. The curves corresponding to different values of ε_1^p are similar in the stress variation region $\sigma_z > \sigma_\varphi$, $\infty < k < 0.93$, as can be seen from Fig. 6. The type of curve $\varepsilon_1^p = 0.2\%$ in the stress variation region $\sigma_z < \sigma_\varphi$ is determined by the Tresk condition. Under repeated simple loadings $\sigma_z = 0.93\sigma_\varphi$, $\sigma_z = 0.75\sigma_\varphi$ yield begins as the stress $\sigma_\varphi(B)$ is achieved at point B. In the same region, the curves $\varepsilon_1^p = 0.5$; 1.0% are similar.

Loading in Accordance with Program 2. Figure 7 shows the loading trajectories. After preliminary loading in trajectory OAB, reverse motion $\sigma_z = \sigma(A)$ into the state of axial tension at point A occurs. Subsequent repeated loadings are complex loadings in straight lines AC at a constant value of the parameter of the type of additional loading: $\mu_{\Delta\sigma} = -1.0$ correspond to line 1 (continuation of the process of simple loading $\Delta\sigma_z > 0$, $\Delta\sigma_\varphi = 0$), $\mu_{\Delta\sigma} = 0.82$, 1.00, 2.00, 3.00, 5.50, 11.00 correspond to lines 2–7 (loading $\Delta\sigma_\varphi > 0$, $\Delta\sigma_z > 0$), and $\mu_{\Delta\sigma} = \infty$ to line 8 (loading $\Delta\sigma_\varphi > 0$, $\Delta\sigma_z = 0$).

The strain diagrams $\sigma_z = \sigma_z(\varepsilon_z)$, $\sigma_\varphi = \sigma_\varphi(\varepsilon_\varphi)$ are shown in Figs. 11 and 12, where 1 are points of the curves in section ABA of the preliminary loading trajectory, and 2 are points of the curve under repeated complex loading in sections AC of the loading trajectory. The experimental data in the sections of complex loading indicate the following.

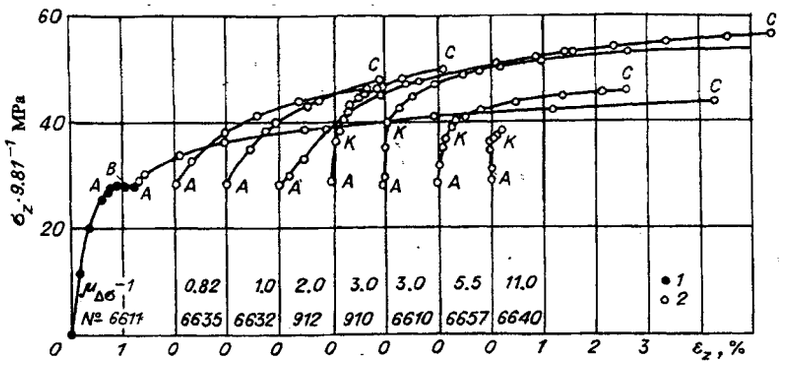

Fig. 11

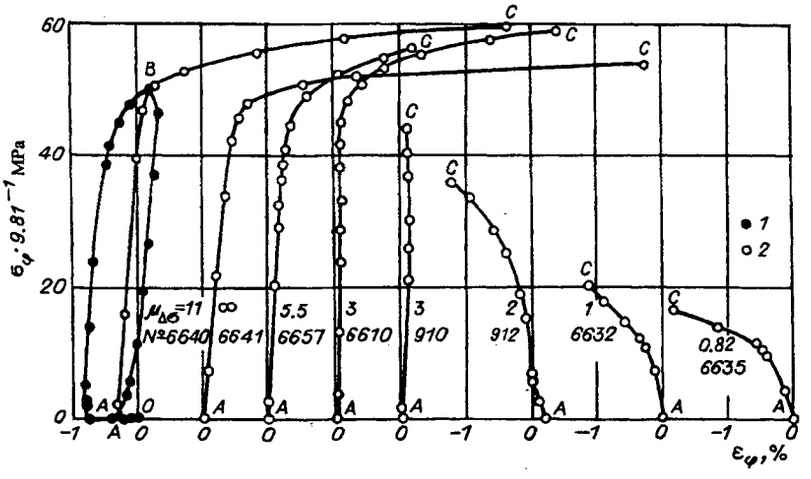

Fig. 12

Additional loadings from point A in sections AC of the loading trajectories at $\mu_\sigma = -1.00$, 0.82, 1.00, 2.00 caused further plastic deformation in the first (axial) and second (circumferential) directions. It is evident from Fig. 12 that a negative increment of the circumferential strain ε_φ corresponds to a positive increment of the circumferential stress σ_φ. This means that whatever the direction of additional loading, which is characterized by the parameter in the form of additional loading $\mu_{\Delta\sigma}$ and by the increment of the maximal tangential stress $2\Delta T = \Delta\sigma_z > 0$, both under active loadings on the sliding areas T, T_{12}, T_{23} ($|\mu_{\Delta\sigma}| \leqslant 1$) and under additional loadings $1 \leqslant \mu_{\Delta\sigma} \leqslant 2$ accompanied by partial unloading in the direction of preliminary plastic deformation T_{12} ($\Delta T_{12} < 0$) and by active loadings on the sliding areas T and T_{23} ($\Delta T > 0$, $\Delta T_{23} > 0$) plastic deformation continues in the same sliding areas T, T_{12} with the loadings in the first section AO of the loading trajectory. No partial strengthening and transition into the deformed state of incomplete plasticity occurs in the direction T_{12}.

The results of the experiment with loadings in section AC at $\mu_{\Delta\sigma} = 3.00$ are shown in Fig. 5, and the mechanism of elastoplastic deformation of the alloy is analyzed in detail above.

The same mechanism of elastoplastic deformation is observed with loadings in sections AC with $\mu_{\Delta\sigma} =$ 5.5, 11.0. With such additional loadings, the slide areas T_{23} become the areas of basic shear. The experimental data in Fig. 12 indicate noticeable plastic deformation in the circumferential direction, which is observed as the stress σ_φ reaches the stress $\sigma_\varphi(B)$ at point B. As can be seen from Fig. 12, a noticeable increase in the limiting deformation in the circumferential direction is observed together with an increase in the strength properties.

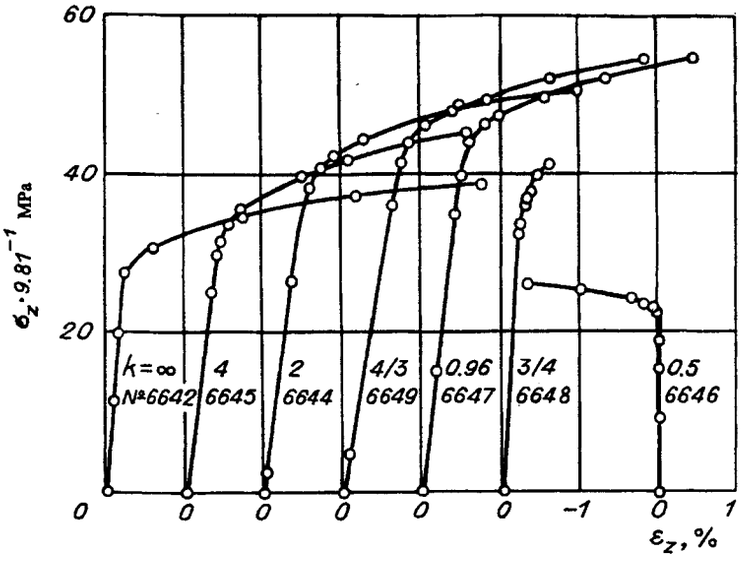

Fig. 13

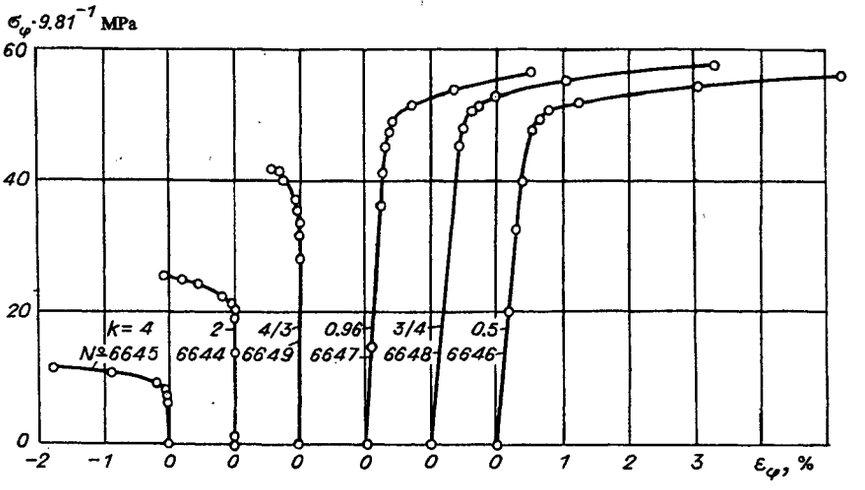

Fig. 14

On the basis of the experimental data in accordance with this program, points of loading surface are marked in the plane of dimensionless variables $\sigma_z/\sigma^s_{0.2} - \sigma_\varphi/\sigma^s_{0.2}$ to tolerances for residual plastic deformation $\varepsilon^p_1 = 0.2,\ 0.5,\ 1.0\%$ under repeated loadings (Fig. 7). For comparison, the dashed line in the figure indicates the initial yield curve. A solid curve is drawn through the points $\varepsilon^p_1 = 0.2\%$. The loading surface shifted in the direction of the ray $\sigma_z = \sigma_\varphi$. In the vicinity of the ray, the yield stress in the axial direction is considerably higher than the yield stress under axial tension; it also exceeds the yield stress under axial tension, on the average, by 20%. The yield stresses in the circumferential direction under additional loadings $\mu_{\Delta\sigma} \geqslant 3$ are close to the value of circumferential stress $\sigma_\varphi(B)$ at point B. The greatest strengthening is observed under additional loadings with $\mu_{\Delta\sigma} = 11.0$. In this case, repeated plastic deformation begins as the stress $\sigma_\varphi(B)$ is reached.

Loading in Accordance with Program 3. Figure 8 illustrates trajectories OAB of preliminary loading, of unloading BOA and repeated loadings–simple loadings realized at the following values of k and μ_σ: $k = \infty$ ($\mu_\sigma = -1$), $k = 4$ ($\mu_\sigma = -0.5$), $k = 2$ ($\mu_\sigma = 0$), $k = 4/3$ ($\mu_\sigma = 0.5$), $k = 0$ ($\mu_\sigma = 1.08$), $k = 3/4$ ($\mu_\sigma =$

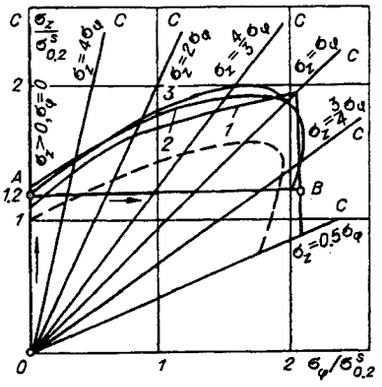

Fig. 15

1.67), $k = 0.5$ ($\mu_\sigma = 3.0$). The strain diagrams $\sigma_z = \sigma_z(\varepsilon_z)$, $\sigma_\varphi = \sigma_\varphi(\varepsilon_\varphi)$ under repeated loadings are given in Figs. 13 and 14. The strain diagrams in sections $OABAO$ of preliminary loading are similar to the diagrams in Fig. 5 (section $OABA$) and in Figs. 9 and 10 (section BO).

The frontal parts of the loading surfaces to tolerances for residual plastic deformation $\varepsilon_1^p = 0.2$, 0.5, 1.0% at repeated loadings are constructed on the basis of the experimental data in Figs. 13 and 14 in the dimensionless plane of the variables $\sigma_z/\sigma_{0.2}^s - \sigma_\varphi/\sigma_{0.2}^s$ (Fig. 8). It follows from the location of the curves that the curves are similar in the domain of stress variation $\sigma_z > \sigma_\varphi > 0$. The dependence of the yield stress on the type of stress is clearly manifested. In the domain of stress variation $\sigma_\varphi > \sigma_z$, the stress $\sigma_\varphi(B)$ at point B at the moment of application of reverse movement can be taken as the yield condition under repeated loadings determined by tolerance $\varepsilon_1^p = \varepsilon_\varphi^p = 0.2\%$.

The dashed line in Fig. 8 shows the frontal part of the initial yield surface. In the domain $\sigma_\varphi < \sigma_z$ the curves of constant values $\varepsilon_1^p = \varepsilon_z^p = \text{const}$ are similar to the initial curve. In the domain of stress variation $\sigma_\varphi > \sigma_z$ the curves $\varepsilon_1^p = \varepsilon_\varphi^p = \text{const}$ agree satisfactorily with the Tresca criterion.

The experimental data in accordance with this program indicate the following. Direct loading OAB, reverse loading BAO, and repeated simple loading OC lead to a change in the loading surface and to its approaching a surface typical of isotropic strengthening in the domain of stress variation $\sigma_z \geqslant \sigma_\varphi \geqslant 0$. In the domain of stress variation $\sigma_\varphi > \sigma_z$, the shape of the surface does not depend on the direction of loading, but is determined only by the stress state achieved (state of complete plasticity, sliding areas T and T_{23}, T_{23} are the areas of basic shear) at point B at the moment of reverse loading application. In the domain of stress variation $\sigma_\varphi > \sigma_z$, plastic shears appear and develop on the same sliding areas T and T_{23} under repeated simple loadings, and T_{23} are the areas of basic shear.

Let us compare the experimental data obtained in loadings in accordance with programs 1–3. Figure 15 illustrates the loading surfaces constructed to tolerance $\varepsilon_1^p = 0.2\%$ (lines 1–3 correspond to loading programs 1–3). The loading surface (line 1) constructed after preliminary complex loading OAB, complete unloading BO, and repeated simple loading OC is located much lower than the surfaces obtained from the data of experiments under programs 2 and 3, in the domain of stress variation $\sigma_z \geqslant \sigma_\varphi \geqslant 0$. The influence of the history of unloading and of subsequent simple or complex loading on the location of the curves is clearly manifested. In the domain of stress variation $\sigma_z < \sigma_\varphi$, the deviation of the curves is insignificant. The loading surfaces have a shape typical of the Tresca yield criterion. The onset of plastic deformation on repeated simple or complex loadings is determined by the stress achieved at point B of the preliminary loading trajectory OAB and does not depend on the history of loading. The initial yield curve is shown in Fig. 15 by a dashed line. The repeated surfaces are located higher than the initial yield curve.

In conclusion, we note the following.

(1) It was found that the shape and dimensions of the loading surface are determined by preliminary plastic deformation which is a result of superposition of the strained states of complete and incomplete

plasticity and complete plasticity with a change of the basic shear areas, by the direction and length of the areas of partial unloading, and by repeated loading under conditions of simple or complex loading.

(2) Anisotropic manifestations of inelastic properties as a result of simple and complex loading accompanied by partial unloading with partial strengthening in the direction of unloading and active loadings in other directions make it possible to use in full the existing reserves of strength and plasticity.

The type of preliminary loading trajectories leading to an increase in the limiting strength and deformation properties in one of the basic directions of the stress tensor in comparison to similar properties in simple loading is determined. The classes of repeated loadings, under which the limiting strength and deformation properties are retained, are specified.

(3) The deformation strengthening of zirconium alloy E-110 under repeated loading is essentially determined by the entire history of preliminary loading, by the history of unloading, and by the direction of repeated loading.

REFERENCES

1. V. M. Zhigalkin and O. M. Usova, "On the reserves of strength in plastic deformation, Communication 1," *Probl. Prochnosti*, No. 11, 3–8 (1991).
2. V. M. Zhigalkin and O. M. Usova, "On the reserves of strength in plastic deformation, Communication 2," *ibid.*, No. 11, 9–13 (1991).
3. E. I. Shemyakin, V. M. Zhigalkin, and G. L. Lindin, "On the question of the reserves of strength in plastic deformation," in: *Strength of Materials and Members in a Complex Stressed State*: Proc. All-Union Conference, Nauk. Dumka, Kiev, (1978), pp. 75–79.
4. E. I. Shemyakin, "Anisotropy of the plastic state," in: *Numerical Methods of Continuum Mechanics*: Collected Scientific Papers [in Russian], Institute of Theoretical and Applied Mechanics, Sibirian Division, Academy of Sceince of the USSR, No. 4, (1973), pp. 150–162.
5. S. A. Khristianovich, "Deformation of a strengthening plastic body," *Izv. Akad. Nauk SSSR, Mekh. Tverd. Tela*, No. 2, 148–174 (1974).
6. L. P. Stepanov, "Time effects in plastic deformation," Candidate's Thesis [in Russian], Moscow (1986).
7. A. V. Nikulina, N. G. Reshetnikov, L. E. Shebaldov, et. al., "Technology for manufacturing channel tubes from alloy Zr–2.5%Nb mounted in RBMK reactors," *Vopr. At. Nauki Tekh., Ser. Materialoved. Novye Mater.*, **2(36)**, 46–54 (1990).
8. B. S. Rodchenkov, E. Yu. Rivkin, A. M. Visnin, et al., "Strength of tubes of technological channels," *ibid.*, 14–21 (1990).
9. G. S. Pisarenko, V. M. Kiselevsky, *Strength and Plasticity of Materials in Radiation Flows* [in Russian], Naukova Dumka, Kiev (1979).
10. A. S. Zaimovsky, A. V. Nikulina, and N. G. Reshetnikov, *Zirconium Alloys in Atomic Power Engineering* [in Russian], Energoatomizdat, Moscow (1981).